


Quartz grain characteristics of the late Pleistocene hard clay in the Yangtze River delta and implications for sedimentary environment and provenance

Chao Wu^{a*} , Peng Qian^{b*}, Xiangmin Zheng^{a*}, Limin Zhou^a, Hui Wang^a, Hongyang Xu^a

^aKey Laboratory of Geo-information Science of Ministry of Education, East China Normal University, Shanghai 200241, China

^bSchool of Geography, Nantong University, Nantong 226007, China

* Corresponding authors e-mail address: 619676293@qq.com (C. Wu); 51163901057@stu.ecnu.edu.cn (X. Zheng); dapeng_96@sina.com (P. Qian).

(RECEIVED April 12, 2019; ACCEPTED March 20, 2020)

Abstract

The sedimentologic fingerprinting in detrital deposit is vital to reconstruct sedimentary environments and discriminate sources. In this study, grain size and microtextural characteristics of quartz from the late Pleistocene hard clay in the Yangtze River delta (YRD) were analyzed by using a laser particle size analyzer and a scanning electron microscope. Subaqueous quartz from the Yangtze River and Yellow River sediments and eolian quartz from the Chinese Loess Plateau loess were also analyzed by scanning electron microscopy to obtain the microtextural characteristics. Quartz grains of the hard clay were characterized by poor sorting, fine skew, bimodal grain-size distributions, and numerous eolian microtextures. The comparison of the quartz grain characteristics of the hard clay with these in eolian loess indicated that the hard clay belonged to an eolian deposition. Moreover, the fine quartz grains of the hard clay were dominated by eolian microtextural characteristics, representing long-distance transportation. The coarse quartz grains of the hard clay exhibited more subaqueous microtextural characteristics, which indicated that the coarse fraction of the hard clay was derived from the proximal source regions in the YRD. The determination of buried eolian deposition with multiple sources in the YRD implies a southward westerly jet stream, strengthened eolian dust transportation, and extensive aridification in the YRD due to the increased Northern Hemisphere ice sheets in Marine Oxygen Isotope Stage 2.

Keywords: Grain-size distribution; Microtextures of quartz silt grains; Eolian deposit; Yangtze River Delta

INTRODUCTION

Eolian dust is not only stored in the form of a loess–paleosol sequence (Ding et al., 2001; Guo et al., 2001; Sun et al., 2006, 2018; Barbara, 2016; Tian et al., 2017; Yan et al., 2017), but also frequently preserved in lacustrine sediments and marine deposits (Zhang et al., 2017, 2018). The latter circumstances represent the complex process of deposition and multiple sources of transportation in the depositional systems of Earth's surface. Therefore, the determination of the eolian deposition and tracing the source of eolian deposits is significant for understanding the sedimentary environment and depositional process (Nie et al., 2015).

The grain-size characteristic analysis of clastic sediments is a valuable sedimentologic method for the identification of sedimentary environments (Zhang et al., 2017). Through the comparison of the results of grain-size characteristics, previous studies have successfully distinguished various clastic sediments from specific sedimentary environments (Sun et al., 2000a). It has also been determined that, due to the stable physical and chemical properties of the quartz grains, grain size can be considered a more precise proxy for the paleoenvironment reconstruction relative to the use of bulk samples (Sun et al., 2000b). Furthermore, fine and coarse components of detrital deposit can be derived from incompatible sources (Kenig, 2006). In recent years, methods of multicomponent separation have been discussed by means of function fitting (Sun et al., 2002; Paterson and Heslop, 2015), end-member modeling (Zhang et al., 2017), and grain-size standard deviations (Boulay et al., 2003). These mathematical methods have achieved satisfactory results in tracing the sources of sediments. Mathematical functions can be effectively used to fit

Cite this article: Wu, C., Qian, P., Zheng, X., Zhou, L., Wang, H., Xu, H. 2020. Quartz grain characteristics of the late Pleistocene hard clay in the Yangtze River delta and implications for sedimentary environment and provenance. *Quaternary Research* 97, 199–215. <https://doi.org/10.1017/qua.2020.31>

grain-size distribution curves and achieve mathematical separation of the grain size components (Sun et al., 2002; Paterson and Heslop, 2015). The grain-size fractions of a sedimentary sequence can be interpreted using integrals and grain-size standard deviations (Boulay et al., 2003).

Microtextural characteristics of quartz grains can be preserved over long periods of time (Kenig, 2006; Costa et al., 2012; Vos et al., 2014; Warrier et al., 2016; Machado et al., 2016; Bellanova et al., 2016; Woronko, 2016). Scanning electron microscopy (SEM) techniques used for sedimentary studies were first improved by Krinsley and Takahashi (1962). Several quartz microtextural characteristics have since been revealed by SEM and essentially applied to interpret a wide range of sedimentologic environments (e.g., eolian, glacial, and subaqueous environments). In addition, quartz microtextural characteristics have also been used as geologic fingerprints in provenance studies (Krinsley and Donahue, 1968; Margolis and Krinsley, 1974; Newsome and Ladd, 1999; Strand et al., 2003; Kenig, 2006; Costa et al., 2012; Vos et al., 2014; Gindy, 2015). Mahaney et al. (2001) provided quantitative techniques for distinguishing various microtextures among various sedimentary environments. A wind tunnel experiment showed relatively short distances and time of eolian transportation were sufficient to create fingerprint features in silica spheres, which indicated that SEM photos were effective tools for researching eolian deposits (Costa et al., 2013). Moreover, based on SEM examination of quartz grains, the finer quartz grains from the Polish loess were probably transported by high winds from a distant area. In contrast, the coarser quartz grains indicated a variable provenance (Kenig, 2006). However, these methods were rarely used in the clastic sediments in China.

It was known that a late Pleistocene hard clay deposit between the Xiashu loess on the west of Yangtze River delta (YRD) and island loess on the East China Sea was distributed throughout the eastern plain of the YRD (Zheng, 1999). The late Pleistocene hard clay layer was determined to be an important marker layer for distinguishing between the Pleistocene and the Holocene (Zheng, 1999). The changes in the thickness of the late Pleistocene hard clay layer, which was the Holocene basement stratum, controlled the extent and process of the Holocene transgression. The formation of the hard clay deposit was controlled by specific climate conditions during the late Pleistocene (Li et al., 2000). Therefore, the hard clay was an important archive for studying the sedimentary environment in the YRD during the late Pleistocene (Li et al., 2000).

The late Pleistocene hard clay was considered to be a continuous stratum distribution with the upper part of the Xiashu loess (Zheng, 1999). As the most important and detailed Quaternary terrestrial archive in subtropical China, the Xiashu loess has been intensively researched and focused upon to explore their origin and provenance and the evolution of the East Asian monsoon (Hao et al., 2010; Qiao et al., 2011; Liu et al., 2014). However, there was a lack of stable sedimentologic evidence to indicate the origin and provenance of the late Pleistocene hard clay. Results from stratigraphy, grain

size, geochemistry, mineral assemblage, microfauna, pollen, and spores, along with the ^{14}C dating, suggested that the late Pleistocene hard clay was an eolian deposition under dry-cold climate conditions during the last glacial maximum (LGM) (Zheng, 1999). However, the high content of freshwater algae indicated that the formation of the hard clay occurred under freshwater environmental conditions (Qin et al., 2008). Therefore, the sedimentary environment of this stratum has not yet been determined, and further investigations are required. Although research on Chinese loess has achieved a series of significant outcomes, many important fundamental questions remain. For example, where is the eastern boundary of the distribution of the Chinese Quaternary loess strata? Is there still distribution of syndepositional eolian deposition of the Xiashu loess in the eastern plain of the YRD? The study of the sedimentary environment and provenance of the late Pleistocene hard clay in the YRD can provide valuable insight into these issues.

In this study, the grain size and microtextural characteristics of quartz, an available weather-resistant mineral in the study area, were analyzed to explore the origin and provenance of the late Pleistocene hard clay in the eastern plain of the YRD. For comparative analysis, the microtextural characteristics of the quartz from Yangtze River sediment, Yellow River sediment, and Chinese Loess Plateau (CLP) loess were also photographed using SEM. The results of this study may potentially provide a significant insight in evolution of the East Asian monsoon and sedimentary patterns of the coast and continental shelf in East China.

MATERIALS AND METHODS

Site description and sample collection

In the research area, the Xiashu loess was widely distributed on the lower slopes, foothills, hillocks, and river terraces of the lower reaches of the Yangtze River, particularly in the Ningzhen Mountain area. The Zhoujia Shan section (ZJS; $32^{\circ}09'49.51''\text{N}$, $118^{\circ}53'43.17''\text{E}$) represented a typical Xiashu loess section (Fig. 1). According to field observations, this section (ca. 6.1 m thick) could be lithologically divided into the following five units: L_a , S_a , L_b , S_b , and L_c (L is the loess unit; S is the paleosol unit) (Fig. 2). In the current study, 61 samples were collected from the ZJS section at 10 cm intervals. The eastern plain of the YRD was covered by unconsolidated Quaternary sediments, with the exception a small number of hills and bedrock in the western area of the YRD (Fig. 1). Multiple drilled boreholes revealed that the stratigraphic distribution and depth of the late Pleistocene hard clay layer in the YRD was generally 20 m underground in the Shanghai area (Zheng, 1999). A 2-m-thick sediment core from the -27 m to -25 m stratigraphic horizons was drilled in the southern area of the YRD ($31^{\circ}11'13''\text{N}$, $121^{\circ}16'2''\text{E}$); the specific site location is shown in Figure 1B. The colors, textures, nodule distribution, and a detailed profile description are listed in Figure 2A. A continuous extensional stratum of the hard clay within the upper part of the

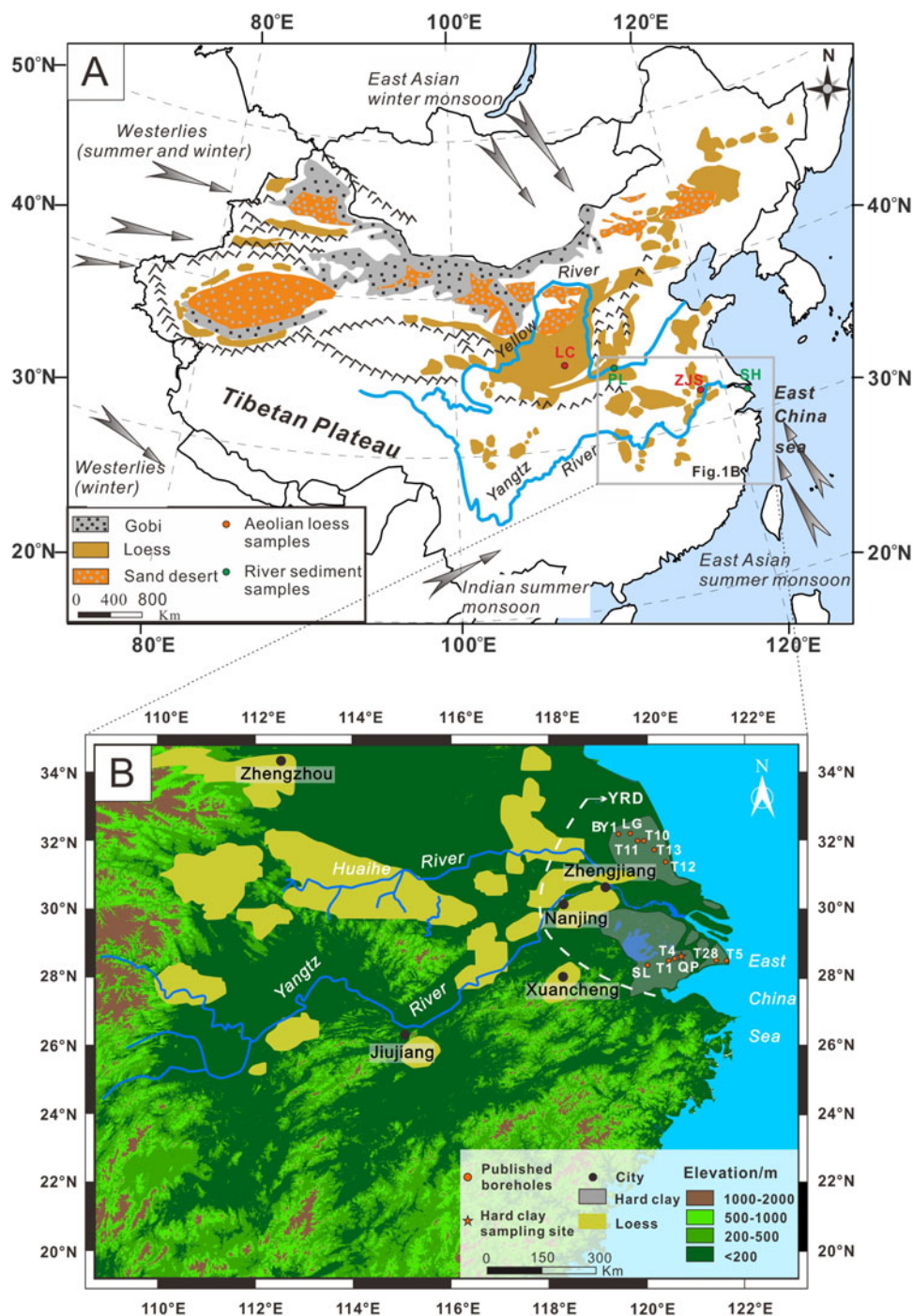


Figure 1. (color online) (A) The mountains, Gobi, sand desert, and loess distributions in China and the locations of samples taken from eolian and subaqueous environments. (B) The distribution of loess in eastern China, hard clay in the Yangtze River delta (YRD), and sampling sites. Digital elevation model of the Yangtze–Huaihe river basin showing regional topographic characteristics. The distribution of loess and hard clay is modified from Qiao et al. (2011) and Zheng (1999). SL core reference from Zheng (1999). T1, T4, T5, T11, T10, T13, T12, and T28 core references from Li et al. (2000) and Chen et al. (2008). BY1 and LG core references from Xia and Zhang (2018).

Xiashu loess section is shown in Figure 2B. The XRD analysis of whole sample of the hard clay indicated that the primary mineral components in the hard clay included quartz, feldspars, magnesioferrite, rutile, hematite, goethite, and muscovite (Fig. 3A). For research purposes, 50 samples of the hard clay were obtained at 4 cm intervals for grain-size analysis. Four samples of the hard clay used to extract quartz

grains were distributed at depths of 2542, 2598, 2646, and 2682 cm. Due to the fact that quartz grain SEM analysis was time-consuming, four samples of the hard clay that were evenly distributed in borehole were used as representative of the sedimentary characteristics of the whole section. The sedimentary characteristics of the samples at depths of 2542, 2598, and 2646 cm were black silty clay with off-white

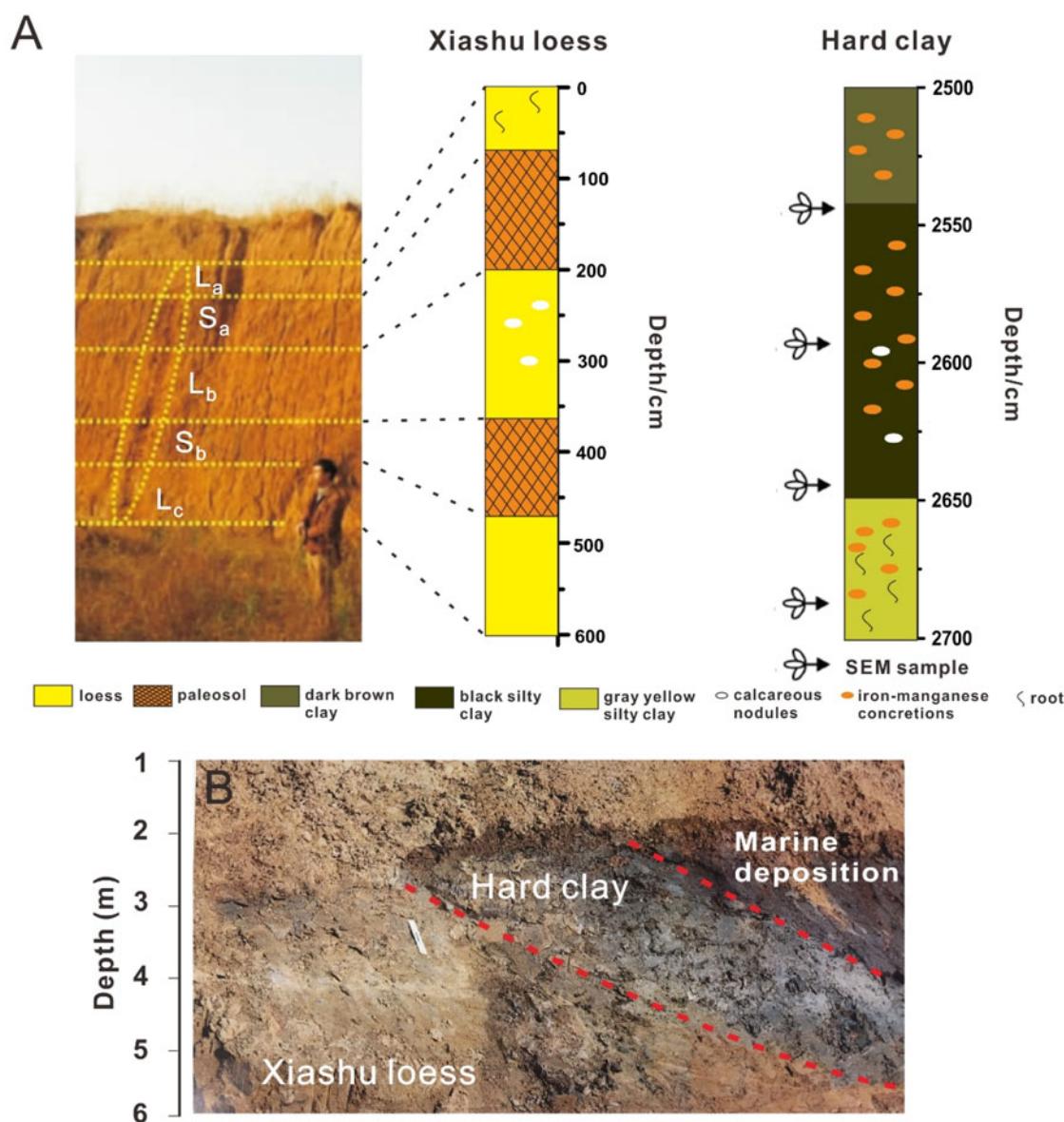


Figure 2. (color online) (A) Lithology of the Xiashu loess in the Zhoujia Shan section (ZJS) and the hard clay core in Shanghai. L, loess unit; S, paleosol unit. (B) The stratigraphic contact relationship of the Xiashu loess and hard clay showing a continuous extensional stratum of the hard clay with the upper part of the Xiashu loess section.

calcareous concretions and iron manganese (Fe-Mn) nodules. The characteristics of the samples at the 2682 cm depth were grayish-yellow silty clay with abundant Fe-Mn nodules and plant roots. For comparative analysis, three samples were collected from the Yangtze River (SH; 31°22'48" N, 121°31'12" E; subaqueous environment), Yellow River (PL; 34°48'30.57"N, 111°10'21.6"E; subaqueous environment), and Chinese Loess Plateau (LC; 35°45'N, 109°25'E; eolian environment) (Fig. 1A).

Quartz single-mineral sample extraction

In this study, the quartz samples were extracted from the separated fractions using a potassium pyrosulfate ($K_2S_2O_7$) fusing-fluorosilicic acid (H_2SiF_6) soaking method (Xiao et al.,

1995) as follows: (1) Approximately 3 g of representative oven-dried samples were treated with 15 mL of 30% H_2O_2 for a 24-hour period to remove the organic matter. (2) The samples were boiled for 4 hours in 50 mL of a 6 mol/L HCl for the purpose of removing the carbonates and iron oxides. (3) Then, 20 g of $K_2S_2O_7$ was added and a 650°C melt was performed for 90 minutes to remove the clay, mica, and layered silicate minerals. (4) The samples were then soaked in a 30% H_2SiF_6 for 3 days with constant stirring to remove the feldspar. (5) At this point, a 9000 rpm centrifugal wash with deionized water was conducted three times, until the water was clear. (6) Finally, the samples were dried at 105°C.

To ensure the effectiveness of the extraction of the quartz minerals, the purity of the quartz samples was tested using

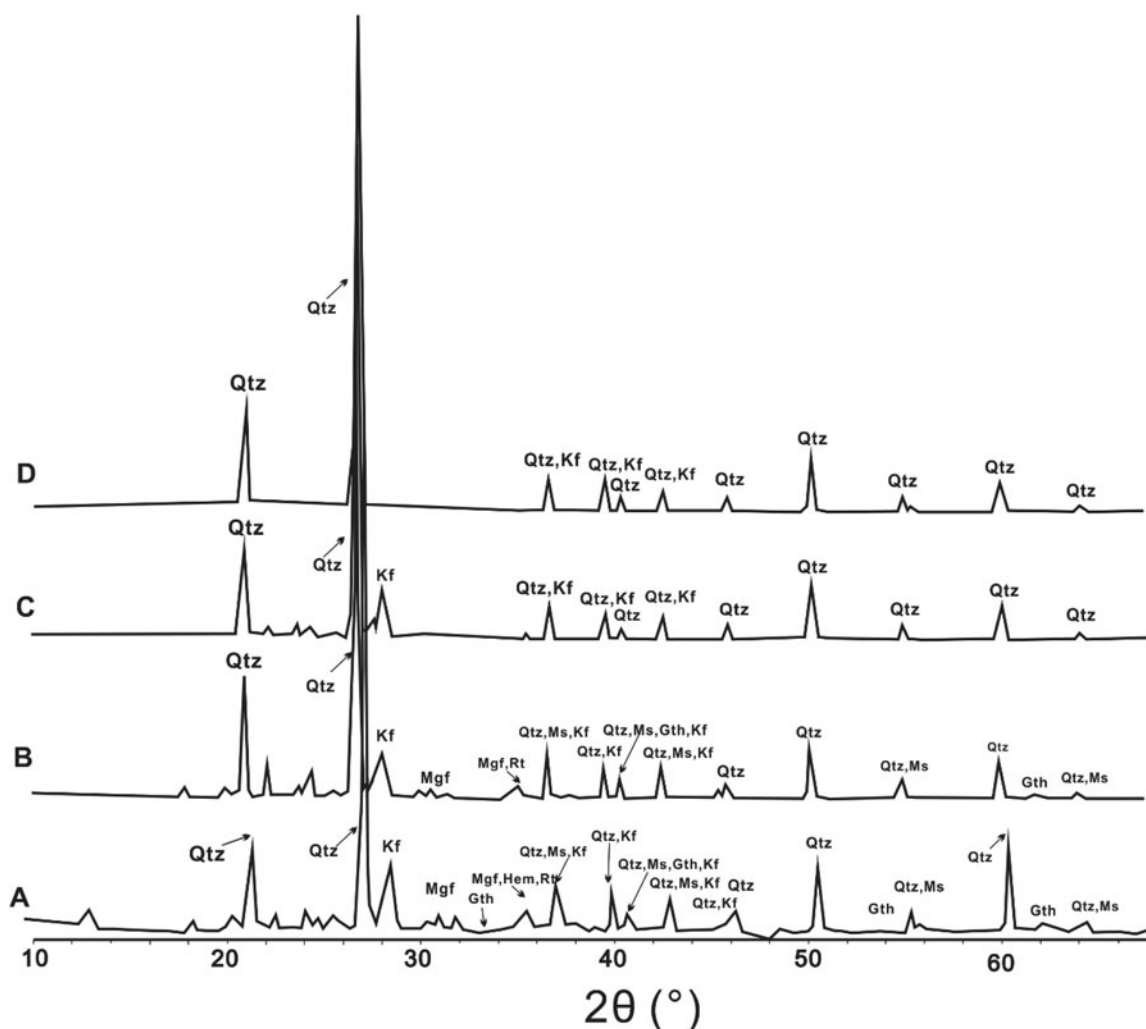


Figure 3. X-ray pattern of samples from different processes of quartz single mineral extraction. (A) The X-ray pattern of original sample of the hard clay. (B) The X-ray pattern of a sample treated with hydrogen peroxide and hydrochloric acid solution. (C) The X-ray pattern of a sample after adding $K_2S_2O_7$ and $650^\circ C$ melt. (D) The X-ray pattern of a sample soaked in a 30% H_2SiF_6 solution for 3 days. Qtz, quartz; Kf, k-feldspars; Mgf, magnesioferrite; Rt, rutile; Hem, hematite; Gth, geothite; Ms, muscovite.

X-ray diffraction (Fig. 3). X-ray diffraction eventually showed only quartz diffraction peaks in the sample (Fig. 3), which demonstrated that we obtained a high-purity quartz sample from the hard clay. The X-ray diffraction test was conducted in the Key Laboratory of Geo-Information Science of the Ministry of Education at the East China Normal University.

Grain size and microtexture of the quartz

In this study's experimental process, 10 mL of $(NaPO_3)_6$ (0.05 mol/L) was added to the quartz samples, and an ultrasonic oscillation was conducted for 10 minutes. The grain sizes were measured using a Master-sizer 2000 laser grain-size analyzer. The measurement error was determined to be less than 2%. Measurement of quartz grain size was conducted at the Geographical Science Department of the East China Normal University.

A cold-field scanning electron microscope (Hitachi S-4800) was used to investigate the microstructures of the

quartz grains. This equipment had the ability to vary the magnification from $20\times$ up to $800,000\times$ to observe the outlines and microtextures on the grain surfaces. The working voltage was fixed at 5 kV; working distance was fixed at approximately 10.6 mm; and the magnification was set from $300\times$ up to $18,000\times$, which successfully guaranteed clear photographs of the quartz grain microtextures. The extracted quartz powder was directly mounted in the metal plate. Metal spraying must be conducted on the surfaces of quartz grains during the test, as quartz is not conductive. Some clay-scale quartz particles adhered to the surfaces of large quartz particles, and the adhesion of these particles can interfere with the observation of the quartz micromorphology, so we chose bright and clean quartz grains to avoid the interference of microparticles during SEM. In this study, the microtextural characteristics of 240 quartz grains from four hard clay samples were statistically analyzed. Because the $<20\ \mu m$ fraction was found to dominate the modern eolian dust (Hao et al., 2010), the quartz particles were simply divided into two

parts (<20 and >50 μm) for statistical purposes. The SEM observation of quartz grains was completed at the electron microscope center of East China Normal University.

Samples of 30 quartz sand grains (>50 μm) from the Yangtze River sediment, 28 quartz sand grains from the Yellow River sediment, and 31 quartz sand grains from the CLP loess were measured to obtain their microtextural characteristics. The roundness and angularity of the quartz grains were identified, referencing the results of Krinsley and Smalley (1973), Kleesment (2009) and Costa et al. (2013). The grain outline represented the roundness and angularity of the grains, which were subdivided into six classes as follows: very rounded, rounded, subrounded, subangular, angular, and very angular (Krinsley and Smalley, 1973; Kleesment, 2009; Costa et al., 2013). The experimental team used the standard atlases of Mahaney (2002), Strand et al. (2003), and Vos et al. (2014) as references during the different microtexture identification processes.

Processing of the granularity data

The grain-size parameters of the quartz grains were calculated using Gradistat software (Blott and Pye, 2001). Grain-size characteristics were based on method of moments calculations. The Folk and Ward method was used to calculate the value of discriminant function parameters. The Sahu discriminant function was $Y = -3.5688 Mz + 3.7016 \sigma^2 - 2.0766 SK + 3.1135 KG$, in which Mz , σ^2 , SK , and KG represented the mean grain size, sorting coefficient, skewness, and kurtosis, respectively (Sahu, 1964). The grain-size standard deviation calculations were derived from the method of Boulay et al. (2003). The curve-fitting method of Sun et al. (2002) was referenced in this study.

Production of wind field patterns in China

The modern wind field pattern in China was plotted based on the NCEP/NCAR reanalysis data set of 2006–2016 (<https://www.esrl.noaa.gov/psd/data/gridded/data.ncep.reanalysis.html>). The wind field pattern of Marine Oxygen Isotope Stage 2 (MIS 2) in China was drawn based on the model result of GISS-E2-R (<https://view.es-doc.org/?renderMethod=name&project=c mip5&client=esdoc-viewer-demo&type=cim.1.software.ModelComponent&name=GISS-E2-R&institute=NASA-GISS>). GISS-E2-R was the NASA GISS atmospheric model (version E2) combined with the Russell Ocean model. Both plots of wind field patterns in China were produced using NCAR Command Language (NCL) mapping software.

RESULTS

Grain-size characteristics of quartz from the hard clay

The coarse and fine component contents in eolian sediment could have been affected by the dynamics of the transport medium, provenance, and sedimentary environment (Lu and An, 1997, 1998). The sand content (>50 μm) of the quartz samples ranged from 2.24 to 30.72%, with an average content of 10.49% (Fig. 4), which was determined to be slightly lower than that in the Xiashu loess (Xu et al., 2016; Supplementary Table S1). The coarse silt content (10–50 μm) of the quartz samples was found to vary from 43.20 to 64.90%, with an average content of 56.72% (Fig. 4), which was determined to be the mode particle group (the most frequently occurring particle group) (Xu et al., 2016; Supplementary Table S1). The fine silt content (5–10 μm) of the quartz samples ranged from 10.34 to 20.87%, with an average content of 15.39% (Fig. 4). The proportion of the clay fraction

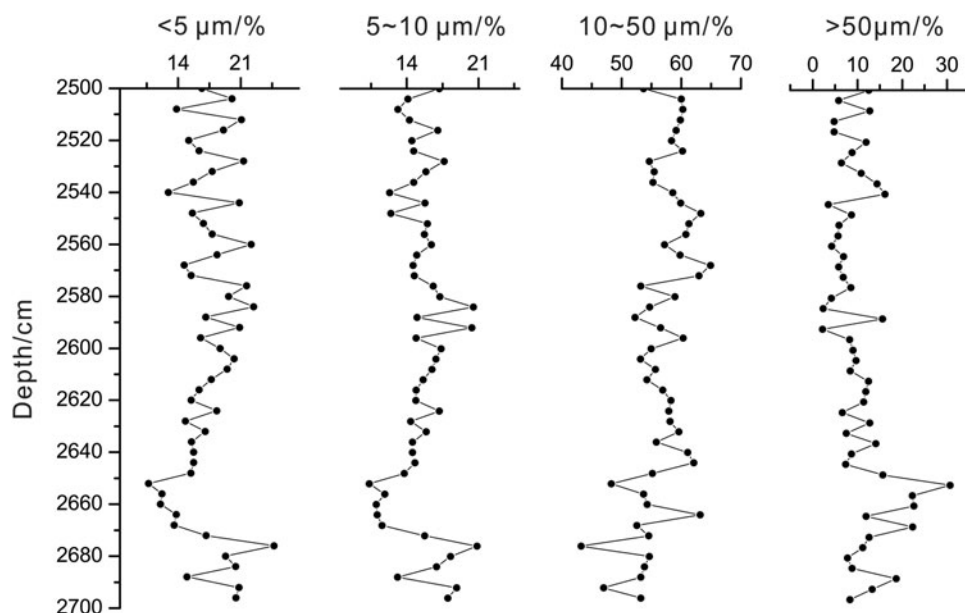


Figure 4. Vertical variation of the quartz grain-size content of the hard clay.

(<5 μm) was between 10.69 and 24.72%, representing the second mode particle group, with an average of 17.41% (Fig. 4).

It was known that the grain-size frequency distribution of a deposit directly reflected the information regarding the grain-size components (unimodal or polymodal) (Lu and An, 1997, 1998). The representative curves of quartz grain-size distributions for the hard clay are illustrated in Figure 5A. It was observed that the grain size of the measured samples ranged from 0.3 to 200 μm with single mode normal distribution. The accumulation curves of quartz grain size reflected the transport modes of a deposition and the sorting under different transportation modes (Lu and An, 1997, 1998). In this study, the cumulative frequency distributions of the quartz grain size for the hard clay were characterized by an “S”-type distribution, which comprised a dominant well-sorted silt fraction (5–50 μm) and a minor poorly sorted clay component (0.3–5 μm) (Fig. 5B). Also, the main transport mode was determined to be suspended transport. The consistency of the quartz grain-size distributions in the hard clay layer indicated that this layer was formed under a single sedimentary dynamic.

The grain-size parameters of sediments, including mean size (Mz), sorting coefficient (Sd), skewness (Sk), and kurtosis (Kg), are closely related to the sedimentary environment and dynamic conditions of transportation (Lu and An, 1997, 1998). The mean size of quartz grains from the hard clay varied from 11.47 to 26.96 μm , with an average of 17.82 μm . The mean size of quartz grains gradually increased from the depth of 2700 to 2650 cm, while this value gradually decreased from the depth of 2650 to 2500 cm. The sorting coefficient ranged from 1.45 to 1.74, with an average of 1.61, indicating poor sorting of the hard clay (Fig. 6). The skewness varied between 0.05 and 1.54, with an average of 0.73, which indicated fine skewed distribution of the hard clay (Fig. 6). The kurtosis ranged from 1.55 to 3.83, with an average of 3.17, showing a mesokurtic distribution of the hard clay (Fig. 6). These findings indicated that the

characteristics of quartz grain from the hard clay were poorly sorted and fine skewed with a mesokurtic distribution.

Microtextural characteristics of the quartz grains

Microtextural characteristics of the quartz grains from the hard clay

Based on identification results, only very angular and angular quartz grains can be observed in the hard clay (Fig. 7). Very angular grains with sharp edges from the four hard clay samples (2542, 2598, 2646, and 2682 cm depths) accounted for 8.7, 44.4, 58.8, and 38.5% of the fine fraction (<20 μm) and accounted for 11.1, 38.5, 50.0 and 69.2% of the coarse fraction (>50 μm), respectively (Fig. 8). Angular grains with sharp edges from the four hard clay samples, accounted for 87.0, 55.6, 35.3, and 61.5% of the fine fraction and accounted for 88.9, 61.5, 50.0, and 30.8% in the coarse fraction, respectively (Fig. 8).

The SEM photographs were visually analyzed and classified according to the presence of 11 main microtextural features on the grain surfaces. These microtextural features were divided into two groups of mechanical and chemical microtextures. Conchoidal fractures (Fig. 7A, HR-1, and YR-3) are typical shell-shaped breakage patterns that mainly show clear arc shapes, as well as the phenomenon of overlapping (Vos et al., 2014; Woronko, 2016). Conchoidal fractures in the four hard clay samples accounted for 17.2, 15.5, 23.5, and 30.8% of the fine fraction (<20 μm) and 11.2, 23.0, 27.8 and 28.8% of the coarse fraction (>50 μm), respectively (Fig. 8). It has been found that arcuate and straight steps (Figs. 7B, CLP-1, and CLP-2) often appear in the intersections between conchoidal fractures and cleavage surfaces and display the characteristics of straight or arc shapes (Vos et al., 2014; Bellanova et al., 2016). In the study, arcuate and straight steps were observed in the fine fraction of the four hard clay samples, in proportions of 21.5, 11.1, 29.3, and

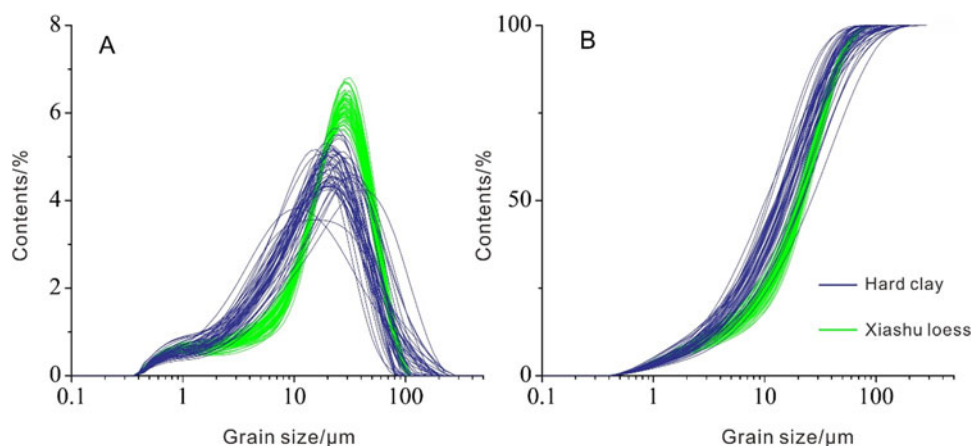


Figure 5. (color online) Comparison of quartz grain-size distributions between the hard clay and the Xiashu loess (Xu et al., 2016). (A) The frequency distribution of grain size. (B) The cumulative frequency distribution of grain size.

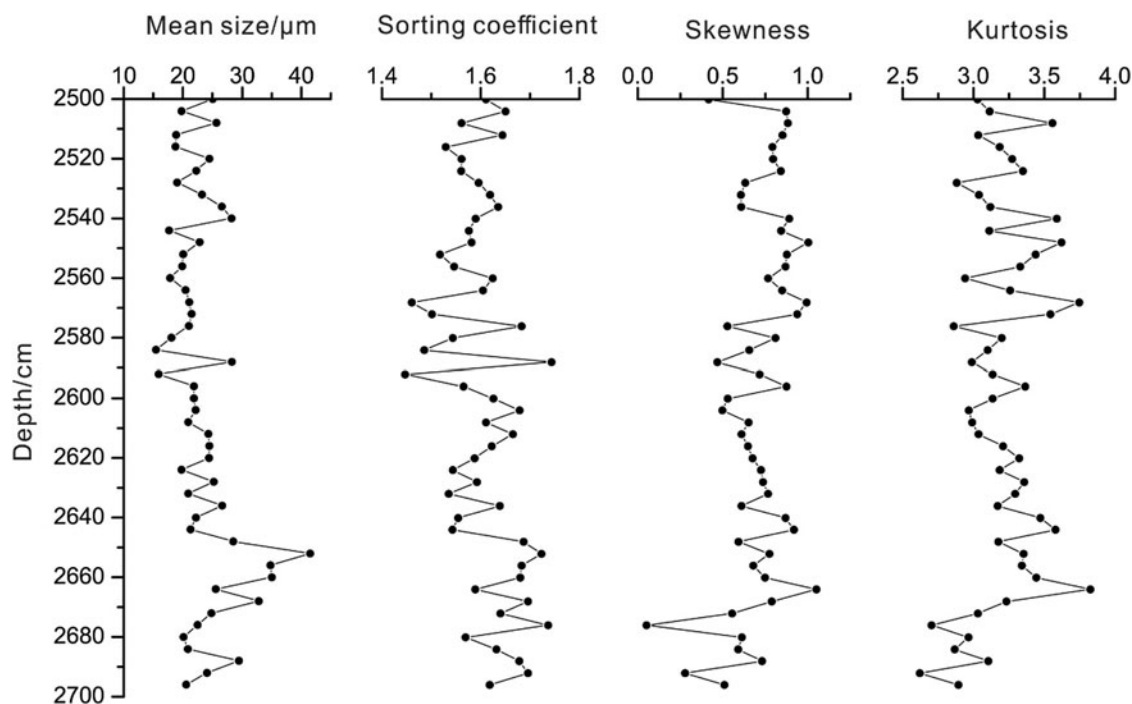


Figure 6. Vertical variation of the quartz grain-size parameters of the hard clay.

23.1%, respectively (Fig. 8). Meanwhile, these microtextures were observed in the coarse quartz grains with the proportions of 21.5, 30.9, 44.6, and 11.0%, respectively. The flat cleavage surfaces (Fig. 7C and CLP-3) are parallel patterns of the cleavage planes, which are known to often occur with flat-shaped fractures (Vos et al., 2014; Machado et al., 2016). The flat cleavage surfaces appeared in the fine fraction of the four hard clay samples at frequency of 21.5, 7.9, 7.3, and 10.1%, while these microtextures rarely appeared in the coarse fraction, at frequencies of 10.7, 0.0, 0.0, and 0.0%, respectively (Fig. 8). The dish pits (Fig. 7D) are saucer-shaped depressions. Dish pits on the coarse quartz grain surfaces from four hard clay samples were observed with percentages of 10.8, 23.2, 12.1, and 23.2%, respectively (Fig. 8). However, these microtextures appeared more frequently on the fine quartz grains, with percentages of 21.6, 39.0, 33.5, and 46.6%, respectively (Fig. 8). The V-shaped percussion cracks (Fig. 7E and 1), triangular-shaped depressions and shallowly indented depressions, have been determined to be the traces of mechanical impacts and wear (Newsome and Ladd, 1999; Kenig, 2006; Vos et al., 2014). The V-shaped percussion cracks were not observed in the fine quartz grains, while these microtextures were observed in the coarse quartz grains, with the proportions of 10.0, 7.9, 5.6, and 7.6%, respectively (Fig. 8). The imbricated grinding features (Fig. 7F) occur as a series of circular or subcircular, hogback-shaped patterns, which have been determined to result from the relative compression between the sharp edges at higher pressures (Costa et al., 2012). This kind of microtexture was only observed in the fine quartz grains from the 2542 cm sample, with the proportion of 11.1%.

Also, as can be seen in Figure 7 CLP-5, meandering ridges appear on the grain surfaces as intersecting lines between the conchoidal fractures (Krinsley and Donahue, 1968; Vos et al., 2014). Meandering ridges on the coarse quartz grain surfaces from the four hard clay samples were observed, with percentages of 8.3, 8.0, 5.8, and 0.0%, respectively (Fig. 8). However, these microtextures appeared more frequently on the fine quartz grains, with percentages of 21.5, 16.9, 15.8, and 15.2%, respectively (Fig. 8). The ditting surfaces (Fig. 7C LP-4 and 2) occur as a series of circular pinholes and are mechanical origin, as distinguished from chemical origin. Ditting surfaces were observed on the coarse quartz grain surfaces from the four hard clay samples, with percentages of 0.0, 11.6, 12.3, and 7.7%, respectively (Fig. 8). However, these microtextures appeared more frequently on the fine quartz grains, with percentages of 8.8, 22.4, 33.9, and 15.4%, respectively (Fig. 8). The polished surface (Fig. 7YR-2) occurs as a smooth flat surface. This microtexture principally appeared on the coarse quartz grains, with percentages of 5.8, 8.5, 7.6, and 8.6%, respectively. These microtextures occurred in inappreciable amounts in the fine quartz grains, with percentages of 9.2, 0.0, 0.0, and 0.0%, respectively. Generally, the frequencies of the flat cleavage surfaces, meandering ridges, dish pits, and ditting surfaces were systematically higher in the fine fractions compared with the coarse fractions. However, the frequencies of the V-shaped percussion cracks and polished surfaces were systematically lower in the fine fractions compared with the coarse fractions.

Apart from the abovementioned mechanical microtextures, several chemical microtextures were observed on the quartz

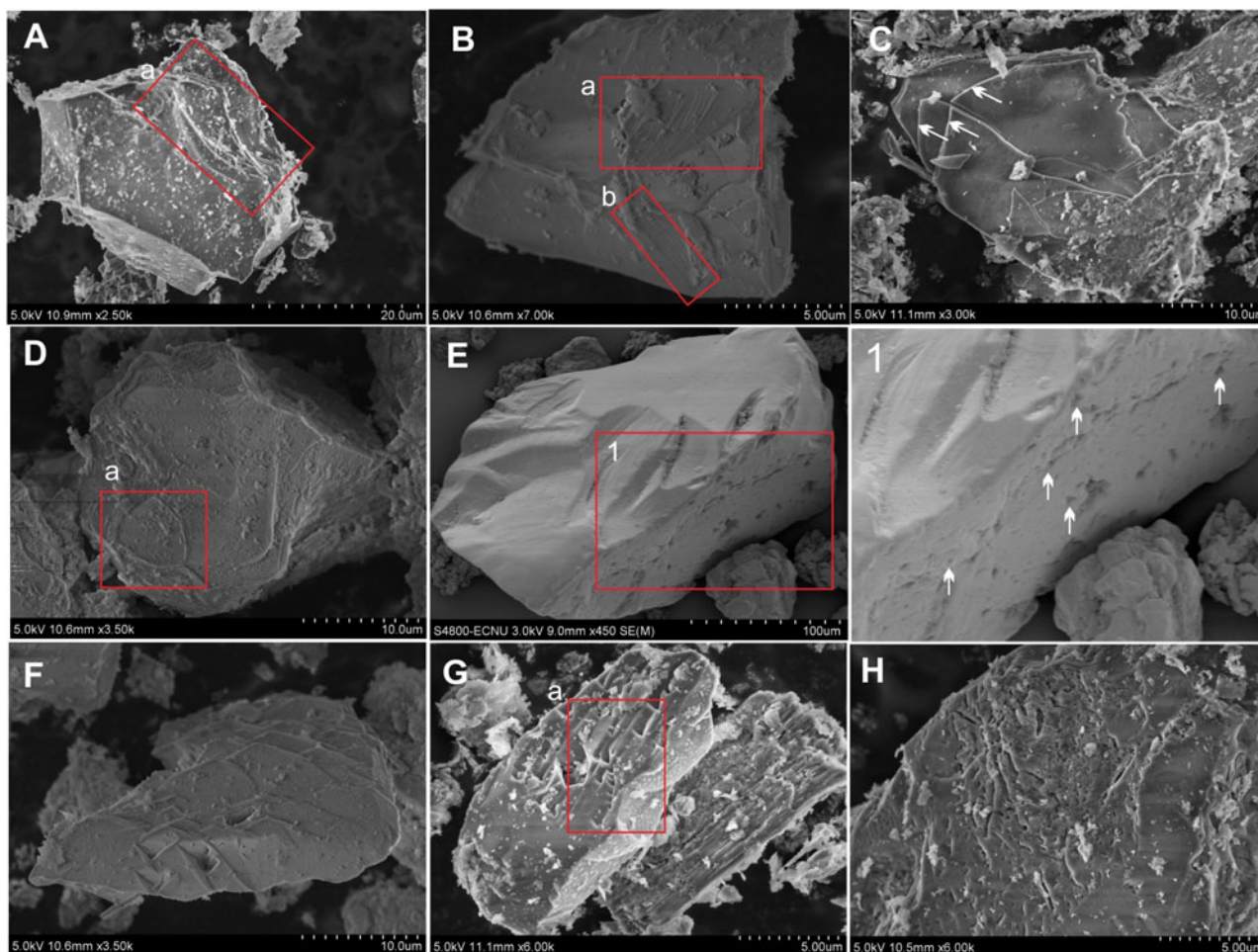


Figure 7. (color online) Quartz grains microtextural characteristics of the hard clay, Yangtze River sediment (YR), Yellow River sediment (HR), and Chinese Loess Plateau (CLP) loess. (A–H) Hard clay quartz grains: (A) Very angular grain with high relief and the presence of a conchoidal fracture (a). (B) Angular grain with medium relief showing an arcuate (a) and straight (b) step. (C) Angular grain with low relief and the presence of a series of flat cleavage surfaces (arrows). (D) Angular grain and the presence of a dish pit (a). (E) V-shaped percussion cracks covering a surface. (1) Enlarged image showing the detail of V-shaped percussion cracks (arrows). (F) Very angular grain with high relief showing imbricated grinding features. (G) Detail of triangular etch pits. The orientation of the etch triangles is extremely regular. (H) Circular solution pits on a fracture plane. (HR-1) A conchoidal fracture. (CLP-1) A straight step. (CLP-2) An arcuate step. (CLP-3) Flat cleavage surfaces. (CLP-4) Ditting surfaces. (2) Enlarged image showing the detail of ditting surface. (CLP-5) Angular grain with low relief showing a meandering ridge (arrows). (YR-1) V-shaped percussion cracks. (YR-2) Polished surface. (YR-3) Surface showing a conchoidal fracture planes (a) with a straight step (b).

grains of the hard clay. Oriented etch pits occur on quartz grains as extremely regular, triangular or rectangular depressions (Fig. 7G). The oriented etch pits appeared in the fine fraction of the four hard clay samples, with frequency percentages of 4.6, 11.1, 5.9, and 15.5%, while these microtextures appeared in the coarse fraction, with percentages of 22.1, 7.8, 5.9, and 7.7%, respectively (Fig. 8). In the study area, it was found that the solution pits (Fig. 7H) display extreme variations in appearance, one example being honeycomb corrosion pits that have developed due to strong chemical erosion. The solution pits appeared in the fine fraction of the four hard clay samples with frequency percentages of 8.9, 5.6, 11.6, and 15.4%, while these microtextures appeared in the coarse fraction with percentages of 11.3, 7.6, 11.2, and 15.4%, respectively (Fig. 8).

Microtextural characteristics of the quartz grains from the Yangtze River sediment, Yellow River sediment, and CLP loess

The frequencies of angular outlines of the coarse quartz grain (>50 μm) from Yangtze River sediment, Yellow River sediment, and CLP loess were 85.7, 76.2, and 36.0%, respectively (Fig. 8). Meanwhile, the very angular coarse quartz grains appeared in these sediments with the proportions of 14.3, 23.8, and 64.0%, respectively (Fig. 8).

The microtextural features of arcuate and straight steps, V-shaped percussion marks, conchoidal fractures, and polished surfaces (Fig. 7) occurred abundantly in the Yangtze River sediment. The frequencies of these microtextural features in the Yangtze River sediment were 50, 35.7, 25, and

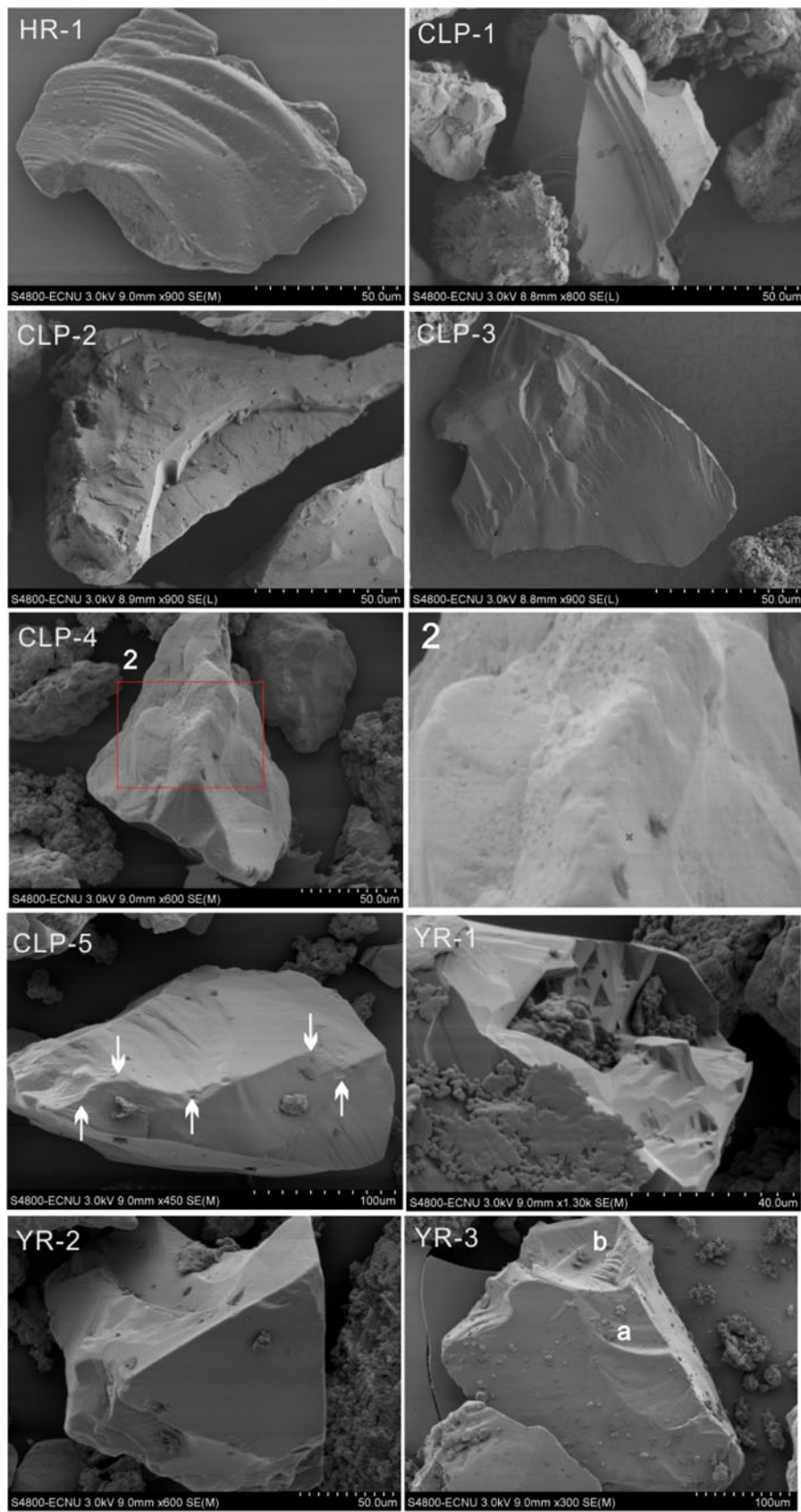


Figure 7. Continued.

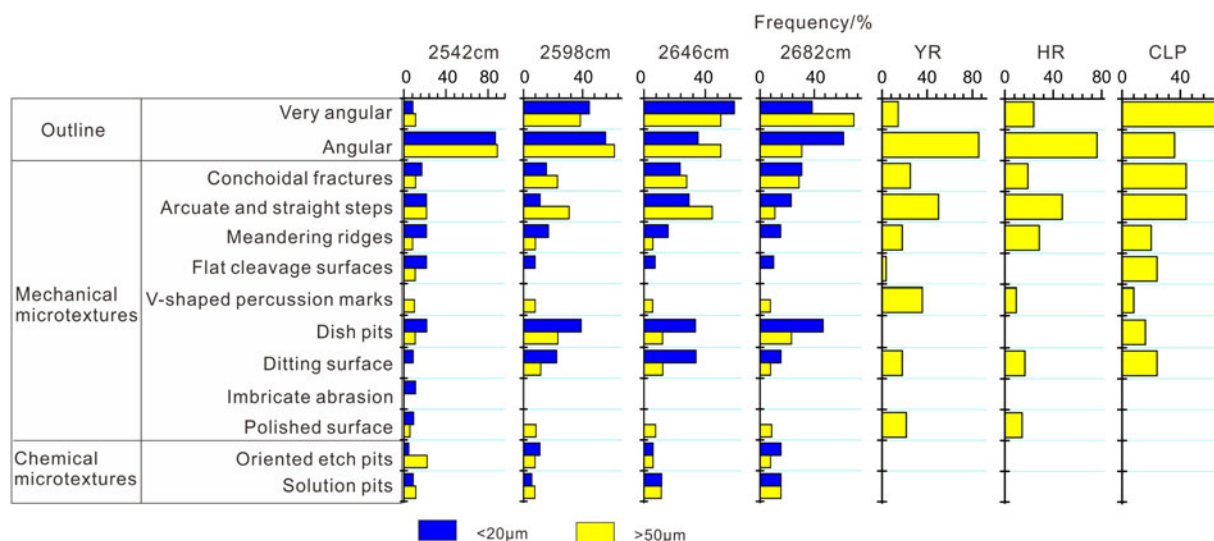


Figure 8. (color online) Frequency histogram of quartz grain microtextural characteristics for the hard clay (2542 cm: $<20\ \mu\text{m}$, $n = 32$; $>50\ \mu\text{m}$, $n = 28$; 2598 cm: $<20\ \mu\text{m}$, $n = 30$; $>50\ \mu\text{m}$, $n = 30$; 2646 cm: $<20\ \mu\text{m}$, $n = 29$; $>50\ \mu\text{m}$, $n = 31$; 2682 cm: $<20\ \mu\text{m}$, $n = 29$; $>50\ \mu\text{m}$, $n = 31$), Yangtze River sediment (YR; $>50\ \mu\text{m}$, $n = 30$), Yellow River sediment (HR; $>50\ \mu\text{m}$, $n = 28$), and Chinese Loess Plateau (CLP) loess ($>50\ \mu\text{m}$, $n = 31$).

21.4%, respectively (Fig. 8). Subsequently, the microtextural features of meandering ridges and ditting surfaces were commonly observed in the Yangtze River sediment. The frequencies of these microtextural features in the Yangtze River sediment were 17 and 17%, respectively (Fig. 8). The microtextural features of flat cleavage surfaces occurred in inappreciable amounts in the Yangtze River sediment with a proportion of 3.5% (Fig. 8). No dish pits, imbricate abrasions, or chemical microtextures appeared in the sand quartz from the Yangtze River sediment (Fig. 8).

The microtextural features of arcuate and straight steps, meandering ridges, and ditting surfaces (Fig. 7) occurred most abundantly in the Yellow River sediment, accounting for 47.6, 28.6 and 28.6%, respectively (Fig. 8). Subsequently, the microtextural features of conchoidal fractures, polished surfaces, and V-shaped percussion marks (Fig. 7) were commonly observed in the Yellow River sediment. The frequencies of these microtextural features in the Yellow River sediment were 19, 14.3, and 9.5%, respectively (Fig. 8). No dish pits, flat cleavage surfaces, imbricate abrasions, or chemical microtextures appeared in the coarse quartz of the Yellow River sediment (Fig. 8).

The microtextural features of conchoidal fractures, arcuate and straight steps, ditting surfaces, and flat cleavage surfaces (Fig. 7) occurred abundantly in the CLP loess. The frequencies of these microtextural features in the CLP loess were 44, 44, 24, and 24%, respectively (Fig. 8). Subsequently, the microtextural features of meandering ridges and dish pits (Fig. 7) were commonly observed in the CLP loess. The frequencies of these microtextural features in the CLP loess were 20 and 16%, respectively (Fig. 8). The microtextural features of V-shaped percussion marks (Fig. 7) were less evident in the CLP loess, with a proportion of 8% (Fig. 8). No imbricate

abrasions, polished surfaces, or chemical microtextures appeared in the coarse quartz of the CLP loess (Fig. 8).

DISCUSSION

The sedimentary environment of the hard clay in the YRD

The analyses of grain-size characteristics have been widely applied in the interpretation of sedimentary environments (e.g. Sun et al., 2006; Wang et al., 2017b). The monomineral of the quartz, relative to the bulk samples, predominantly represented the grain-size characteristics of the original dust, due to the fact that a relatively small alteration occurred for quartz grains during the process of postdeposition pedogenesis (Sun et al., 2000b). In this study, the quartz grain-size distributions from typical eolian loess presented the characteristics of a positive skew (e.g., toward the finer sizes) and bimodal distribution. However, there was a pronounced mode observed in the 20 to 40 μm fraction (Sun et al., 2000a; Xu et al., 2016). The quartz grain-size distribution of the hard clay was a bimodal distribution, with a fine tail and a dominant peak. The silt fraction in the hard clay accounted for the high proportion. These features were found to be very similar to the typical loess and indicated that the hard clay had the characteristics of an eolian deposit. Also, a sedimentary environment could be inferred from the Sahu discriminant function value of Y (Sahu, 1964). It was determined that the negative value of Y represented the eolian sediment, while its positive value represented the subaqueous sediment. Figure 9 illustrates the fact that the Y values of the hard clay are all negative, which suggests that the hard clay belongs to an eolian deposit.

The meandering ridges were confirmed to be distinct properties of eolian transportation in desert and littoral dunes (Krinsley and Donahue, 1968; Vos et al., 2014). Conchoidal fractures commonly occurred in the microtextures of quartz grains and were produced in a wide range of environments. If the conchoidal fractures were more uniform in size and generally less than 10 μm , these characteristics indicated an eolian and littoral environment (Vos et al., 2014; Woronko, 2016). The formation of flat cleavage surfaces was a prominent feature of quartz grains and has been attributed to eolian and glacial environments (Krinsley and Donahue, 1968; Krinsley and Cavallero, 1970; Mahaney, 2002; Costa et al., 2013). It was clear from the microtextural results of the wind tunnel experiment conducted by Costa et al. (2013) that the predominantly fresh surfaces, fractures, and abrasions increased with increasing time and wind velocities. These microtextural features under eolian environments were also supported by the investigation of the CLP loess. The microtextural features of meandering ridges, conchoidal fractures, flat cleavage surfaces, and ditting surfaces were frequently observed in the CLP loess (Fig. 8). In the study area, these microtextural characteristics of the quartz grains under an eolian environment were observed on the quartz grain surfaces as high frequencies. These features imply that the original dust that formed the hard clay had an eolian history.

The clastic sediments had generally undergone a process of production and were transported by a series of geologic agents before deposition in the accumulation area. The detrital zircon U-Pb age revealed that the northeastern margin of the Tibetan Plateau was an important source area of loess in the CLP. However, the detrital material was transported through the Yellow River to the floodplain in the middle reaches of the Yellow River, then transported by the East Asian winter monsoon, and deposited on the CLP (Nie et al., 2015). In addition, abundant materials from the CLP were eroded into the Yellow River. Therefore, apart from the microtextural features of the subaqueous environment, rich microtextural features, for example, meandering ridges

and ditting surfaces, which were formed under an eolian environment, also were observed in the quartz grains from Yellow River (Fig. 8).

The depositional process of the hard clay was found to be complicated due to the presence of microtextural characteristics of imbricated grinding features, V-shaped percussion cracks, and arcuate and straight steps. Arcuate and straight steps are one of the most frequently observed features in glacial deposits (Strand et al., 2003). Moreover, imbricated grinding features are only observed on glacial grains and have been used diagnostically for the identification of glacial grinding (Margolis and Kennett, 1970). It is known that V-shaped percussion cracks are produced mainly through impacts in highly energetic subaqueous environments (Mahaney and Kalm, 2000). In the present study, based on the abovementioned various microtextural characteristics of quartz grains, it was found that the quartz grains in hard clay had experienced considerably long-term supergene geologic processes before they were associated with the hard clay accumulation. In summary, the quartz grain characteristics of the hard clay indicated an eolian history. In this study, two situations were proposed: (1) The dust had been transported by the wind directly from its provenance to the deposition area; or (2) the original materials were first transported by glacial or fluvial processes into the sedimentary system, and then blown by the wind into the accumulation zone. The eolian signal contained in the hard clay directly indicated the dry and cold sedimentary environment in the YRD during the late Pleistocene. In previous studies, the study of sporopollenin showed that the low content of sporopollenin fossils and herbs in the hard clay layer reflected a cold climate (Qin et al., 2008). The spore combinations of gramineae–cyperaceae, defoliation–pine–artemisia, and sedge–deciduous–palm indicated that vegetation patterns on the YRD and surrounding mountains were meadows, coniferous forests, and broad-leaved mixed forests, respectively (Qin et al., 2008).

The multiple provenances of the hard clay in the YRD

In a previous study, Zheng (1999) discovered and confirmed that the hard clay was a continuous extensional stratum of the Xiashu loess (Fig. 2B). The Xiashu loess was considered as a continuation of the CLP loess due to the similar grain-size characteristics (Zheng, 1999) and geochemical compositions (Zhang et al., 2007; Mao et al., 2011). During a period ranging from March 26 to March 27, 2000, severe dust storms originating from the arid areas of northern China reached the Shanghai area (Shi et al., 2006). The modern meteorological data suggested that the fine-particle fractions of the clastic sediments in the YRD could have been derived from the arid areas of the northern China (Zheng, 1999; Chow et al., 2014). The degree of drought and desertification last strengthened in northern China during the late Cenozoic and provided sufficient material sources for the loess deposits in eastern China (Guo et al., 2004). In the present study, when a mass of eolian dust was transported from northern China to eastern China during the late Pleistocene, it was concluded that the

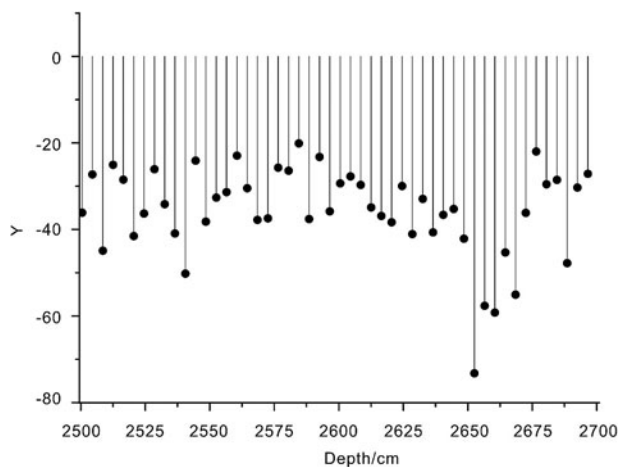


Figure 9. The Y value diagram of sedimentary environment discrimination.

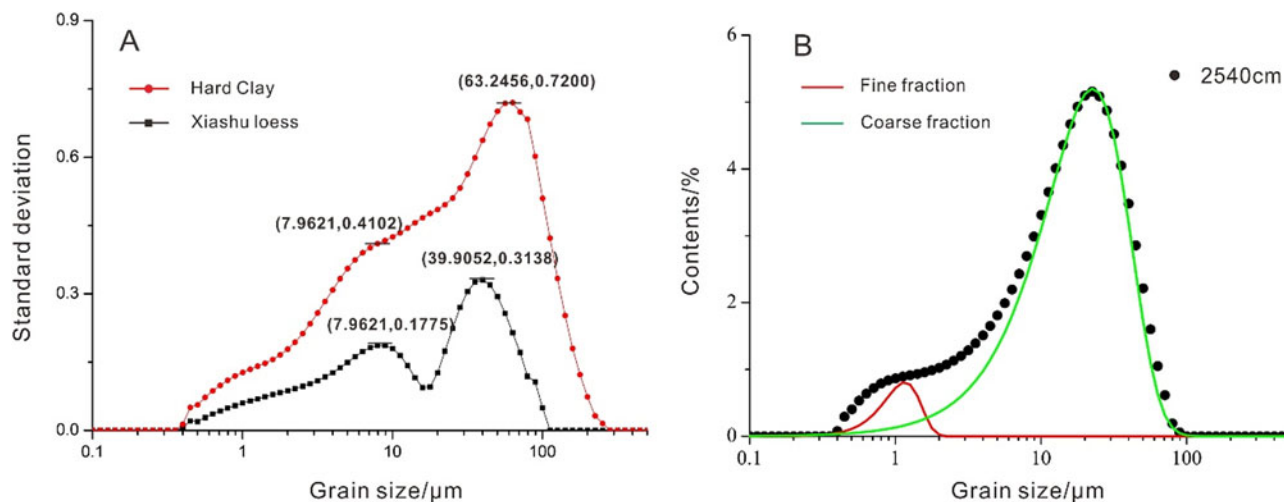


Figure 10. (color online) (A) Grade standard deviation curve of the quartz grain size of the hard clay and the Xiashu loess. (B) The grain-size distribution of the 2540 cm sample. This curve was fit using a Weibull function with two peaks following Sun et al. (2002).

eolian dust would most likely have been stored in the YRD. In other words, the arid area of the northern China was an important potential source area for the late Pleistocene hard clay deposition.

The microtextures on quartz surfaces can be used as “fingerprints” to trace sediment provenance through detailed comparison with potential sources (Wang et al., 2017a). The quartz grain microtextural characteristics of the Xiashu loess mainly included the mechanical characteristics of dish pits, conchoidal fractures, flat cleavage surfaces, breakage blocks, striations, and ditting surfaces (Xu et al., 2016). The eolian microtextural features of meandering ridges, conchoidal fractures, flat cleavage surfaces, and ditting surfaces were abundant in the CLP loess. The micromorphology features of the quartz grains, such as dish pits, meandering ridges, flat cleavage surfaces, and ditting surfaces appeared at high frequencies in the fine fraction (<20 μm) of hard clay and are considered as the results of long-transportation by wind. According to the results of the simulations and observations of eolian transportation, the <20 μm fraction of eolian dust could be suspended over long distances (Pye, 1987). The quartz grain-size fractions of <20 μm in the hard clay accounted for more than 50%, respectively, as shown in Figure 5B. Although the silt-size aggregates in the loess were able to be lifted to form aerosol particles (Jeong, 2008), we suggest that the amount of this component was small. Taking into consideration both aerodynamic laws and microtextures, it was concluded that the fine fraction of the hard clay had been transported from a distant area.

As discussed by Pye (1987), the 20 to 70 μm fractions of the eolian dust were short-term suspensions. In a comparison of the grain-size fractions of typical CLP loess (Sun et al., 2002; Vandenberghe, 2013) and Xiashu loess (Xu et al., 2016), it was suggested that the sand fraction (>50 μm) of the hard clay, with a proportion of less than 30%, was unlikely to have undergone long-distance transport by wind. After removing the impact of the postdepositional

pedogenesis, the average sorting value of the quartz grains was determined to be 1.60 for the hard clay, which was higher than that of the CLP loess (1.23) and Xiashu loess (1.59), respectively (Sun et al., 2000a; Xu et al., 2016). In other words, since driven by the East Asian winter monsoon, the sorting of the dust became worsened (more random) with the increasing transportation distance, indicating that material from additional sources was mixed in during the process of the dust transportation.

In the present study, an obvious view of the statistical data for the four samples was that the coarse fraction, relative to the fine fraction, provided more of the surface micromorphology characteristics under subaqueous environments (for example, V-shaped percussion cracks and polished surfaces). These findings suggest that the coarse and fine quartz fractions in the hard clay had different provenances. Although the source of the Xiashu loess remained not entirely clear, increasing amounts of evidence indicated that near-source materials were mixed into the Xiashu loess (Hao et al., 2010; Qiao et al., 2011; Liu et al., 2014). Therefore, we conclude that the coarse fractions of the hard clay were preferentially derived from proximal source regions of the Yangtze River basin. This conclusion was consistent with the results of the U-Pb age spectrum of the >40 μm detrital zircons in the Xiashu loess (Liu et al., 2014). Our conclusion concerning a proximal source for the coarse fraction in hard clay is also supported by the subaqueous microtextural features (V-shaped percussion cracks and polished surfaces) which were found to be abundant in the Yangtze River sediment (Fig. 8).

The multipeak curves of grade standard deviations indicated that the grain-size distributions of sediments are controlled by multiple factors (Boulay et al., 2003). Figure 10A shows that the curve of the quartz grade standard deviation of the hard clay is a bimodal distribution, which was determined to be the result of different provenances or depositional dynamic change. The previous analyses had basically

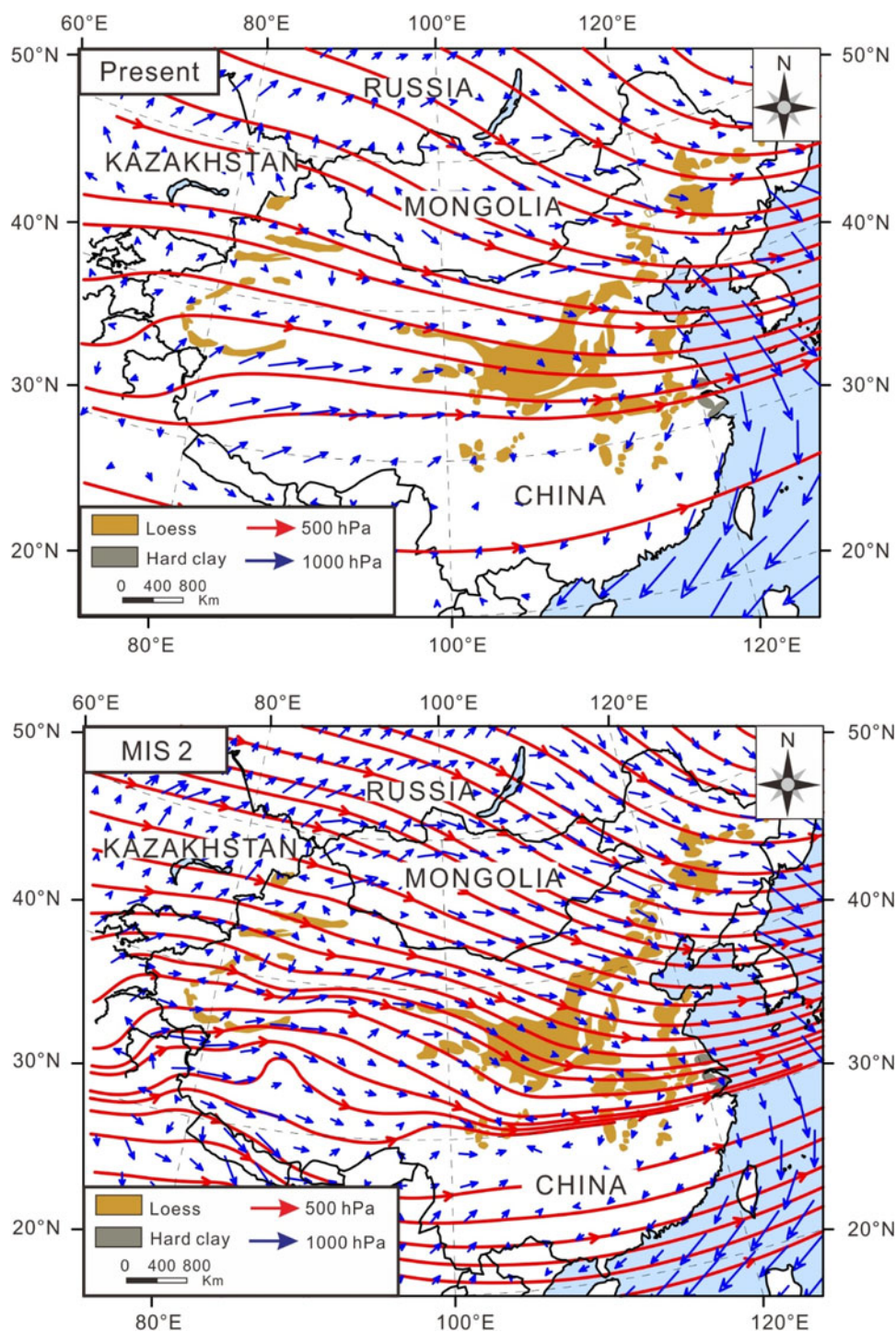


Figure 11. (color online) Top, The modern wind field pattern of winter (December, January, February) in China. This wind field pattern is drawn based on the NCEP/NCAR reanalysis data set of 2006–2016. Bottom, The pattern of winter monsoon and subtropical jet during Marine Oxygen Isotope Stage 2 (MIS 2) in China. The wind field pattern of MIS 2 is drawn based on the model result of GISS-E2-R (last glacial maximum).

eliminated the influences of the various depositional dynamics. Eventually, a bimodal distribution of the grade standard deviation curve indicated the existence of two provenances for the hard clay in the study area. The grain-size distributions of sediment with certain dynamic distributions are the results of single-factor random events under the same transport

mode. Furthermore, the digital characteristics of grain-size distributions of sediments obey a type of mathematical distribution (Sun et al., 2002; Paterson and Heslop, 2015). As shown in Figure 10B, the two peaks of grain-size frequency distributions were separated by using the Weibull function, which indicated that the hard clay had multiple

sources. As detailed in Figure 11, the China winter wind field showed that the eolian sedimentary system was mainly affected by the upper westerly jet stream, near-surface East Asian winter monsoon. Recently, loess-like deposits in the Pearl River delta area that may have been derived from north-western China were reported (Wang et al., 2015). In the Northern Hemisphere westerlies, the fine dust derived from central Asian desert was transported to the CLP (Sun et al., 2013), Japan (Yamamoto et al., 2013), the North Pacific (Zhang et al., 2016), and the Greenland ice core (Bory et al., 2003) by upper-level westerly jet stream. Combined with the findings presented earlier and the data shown in Figure 11, the results of this study suggest that the fine-grain fraction of the hard clay was related to the Northern Hemisphere westerlies (Sun et al., 2000a). However, the coarse fractions of the hard clay were transported by the East Asian winter monsoon.

The sedimentary age and controlling factors of the hard clay in the YRD

Based on the ^{14}C dating of the shell fragments in the overlying marine deposition of the hard clay, the samples taken from T1, T4, T28, and T5 yielded ages of 7.06 ± 0.3 , 8.23 ± 0.3 , 14.19 ± 0.22 , and 10.17 ± 0.3 ^{14}C ka BP, respectively (Chen et al., 2008; Li et al., 2000). Our ^{14}C dating of the shell fragments in the overlying and underlying marine deposition of the hard clay in the Shanglin (SL) core determined the ages to be 7.37 ± 0.14 and 28.8 ± 0.54 ^{14}C ka BP, respectively (Zheng, 1999). For the hard clay layer distributed on the northern part of the YRD, the ages at the bottom (BY1 core) and middle (LG core) of the hard clay were 26.5 ± 0.06 and 1.39 ± 0.39 ^{14}C ka BP, respectively (Xia and Zhang, 2018). The age of the overlying marine deposition of the hard clay at T11, T10, T13, and T12 was 7.76 ± 0.3 , 12.8 ± 0.35 , 14.83 ± 0.39 , and 11.78 ± 0.37 ^{14}C ka BP, respectively (Chen et al., 2008; Li et al., 2000). In conclusion, the deposition of hard clay in this study occurred approximately from 25 to 12 ka BP. The formation of this hard clay layer was related to specific environmental conditions.

During the hard clay sedimentary period (from 25 to 12 ka BP) (Zheng, 1999), which corresponded with the LGM stage, there was an important global dry-cold event (Heinrich, 1988). The occurrence of LGM was revealed by $\delta^{18}\text{O}$ record of Greenland ice core between Heinrich events 2 and 1 (abrupt cooling climate events), approximately 24–18 ka BP (Heinrich, 1988). Song et al. (2018) indicated that cooling climate signals corresponding to Heinrich events may have been transmitted from central Asia to the East Asian monsoon areas by the Northern Hemisphere westerlies. Due to an increased volume of ice sheets in Greenland and the polar region, the Mongolian and Siberian Highs then intensified, which led to enhanced winter monsoons, along with a southward shift in the westerly jet stream, as seen in the Figure 10 during MIS 2 (Ding et al., 1995; Liu et al., 1999; Tian et al., 2017). We consider that the cooling events leading to enhanced East Asian winter monsoon, southward shift in the westerly jet stream,

and aridification of source and deposition areas may have controlled the formation of the late Pleistocene hard clay in the YRD.

CONCLUSIONS

The similarities of the quartz grain size between the hard clay and the typical eolian loess indicated that the hard clay had the characteristics of an eolian deposition. Moreover, the quartz micromorphology characteristics of the hard clay provided information regarding the eolian history for the hard clay. In comparison with the fine quartz grain microtextures, the coarse quartz grains exhibited more pronounced microtextures under a subaqueous environment, which suggests that the fine and coarse fractions of the hard clay were derived from different source areas. The grain-size distributions and grade standard deviation curve of the quartz grains from the hard clay revealed the existence of multiple provenances for the hard clay. In combination with the modern meteorological data and quartz grain characteristics, this study proposes that the fine and coarse fractions of the hard clay were related to the Northern Hemisphere westerlies and East Asian winter monsoons, respectively. The late Pleistocene hard clay deposition with multiple provenances in the YRD was a result of the southward westerly jet stream, strengthened East Asian winter monsoon, and extensive aridification when the volume of Northern Hemisphere ice sheets was increased during MIS 2.

ACKNOWLEDGMENTS

This work was financially supported by the China Natural Science Foundation (grant nos. 41871015 and 41671003) and the East China Normal University Academic Innovation Promotion Program for Excellent Doctoral Students (grant no. YBNLTS2019-002).

SUPPLEMENTARY MATERIAL

The supplementary material for this article can be found at <https://doi.org/10.1017/qua.2020.31>

REFERENCES

- Barbara, A.M., 2016. Palaeoclimatic records of the loess/palaeosol sequences of the Chinese Loess Plateau. *Quaternary Science Reviews* 154, 23–84.
- Bellanova, P., Bahlburg, H., Nentwig, V., Spiske, M., 2016. Microtextural analysis of quartz grains of tsunami and non-tsunami deposits—a case study from Tirúa (Chile). *Sedimentary Geology* 343, 72–84.
- Blott, S.J., Pye, K., 2001. GRADISTAT: a grain size distribution and statistics package for the analysis of unconsolidated sediments. *Earth Surface Processes and Landforms* 26, 1237–1248.
- Bory, A.J.M., Biscaye, P.E., Grousset, F.E., 2003. Two distinct seasonal Asian source regions for mineral dust deposited in Greenland (NorthGRIP). *Geophysical Research Letters* 30(4).
- Boulay, S., Colin, C., Trentesaux, A., Pluquet, F., Bertaux, J., Blamart, D., Buehring, C., Wang, P., 2003. Mineralogy and sedimentology of Pleistocene sediments on the South China Sea (ODP Site 1144). In: Prell, W.L., Wang, P., Blum, P., Rea,

- D.K., Clemens, S.C. (Eds.), *Proceedings of the Ocean Drilling Program: Scientific Results*. Vol. 184. Ocean Drilling Program, Texas A&M University, College Station, pp. 1–21.
- Chen, Q.Q., Li, C.X., Li, P., Liu B.Z., Sun, H.P., 2008. Late Quaternary palaeosols in the Yangtze Delta, China, and their palaeoenvironmental implications. *Geomorphology* 100, 465–483.
- Chow, K.C., Su, L., Fung, J.C., Ma, H., Lau, A.K., 2014. Numerical modeling of a strong dust event over the south China region in March 2010. *Meteorology and Atmospheric Physics* 126, 119–138.
- Costa, P.J.M., Andrade, C., Dawson A.G., Mahaney W.C., Freitas M.C., Paris R., Taborda R., 2012. Microtextural characteristics of quartz grains transported and deposited by tsunamis and storms. *Sedimentary Geology* 275–276, 55–69.
- Costa, P.J.M., Andrade, C., Mahaney, W.C., Marques da Silva, F., Freire, P., Freitas, M.C., Janardo, C., Oliviera, M.A., Silva, T., Lopes, V., 2013. Aeolian microtextures in silica spheres induced in a wind tunnel experiment: comparison with aeolian quartz. *Geomorphology* 180–181, 180–129.
- Ding, Z., Liu, T., Rutter, N., Yu, Z., Guo, Z., Zhu, R., 1995. Ice-volume forcing of East Asian winter monsoon variations in the past 800,000 years. *Quaternary Research* 44, 149–159.
- Ding Z.L., Yu Z.W., Yang S.L., 2001. Coeval changes in grain size and sedimentation rate of eolian loess, the Chinese Loess Plateau. *Geophysical Research Letters* 28, 2097–2100.
- Gindy, N.N., 2015. Environmental implications of electron microscope study of quartz grains' surface textures on khors sediments, Lake Nasser, Egypt. *Egyptian Journal of Aquatic Research* 41, 41–47.
- Guo Z.T., Peng S.Z., Hao Q.Z., 2001. Origin of the Miocene–Pliocene red-earth formation at Xifeng in Northern China and implications for paleoenvironments. *Palaeogeography, Palaeoclimatology, Palaeoecology* 170, 11–26.
- Guo, Z.T., Peng, S.Z., Hao, Q.Z., Biscaye, P. E., An, Z.S., Liu, T.S., 2004. Late Miocene–Pliocene development of Asian aridification as recorded in an eolian sequence in northern China. *Global and Planetary Changes* 41, 135–145.
- Hao, Q.Z., Guo, Z.T., Qiao, Y.S., Xu, B., Frank, O., 2010. Geochemical evidence for the provenance of middle Pleistocene loess deposits in southern China. *Quaternary Science Reviews* 29, 3317–3326.
- Heinrich, H., 1988. Origin and consequences of cyclic ice rafting in the Northeast Atlantic Ocean during the past 130,000 years. *Quaternary Research* 29, 142–152.
- Jeong, G.Y., 2008. Bulk and single-particle mineralogy of Asian dust and a comparison with its source soils. *Journal of Geophysical Research* 113(D2).
- Kenig, K., 2006. Surface microtextures of quartz grains from Vistulian loesses from selected profiles of Poland and some other countries. *Quaternary International* 152–153, 118–135.
- Kleesment, A., 2009. Roundness and surface textures of quartz grains in Middle Devonian deposits of East Baltic and their palaeogeographic implications. *Estonian Journal of Earth Science* 58, 71–84.
- Krinsley, D.H., Cavallero, L., 1970. Scanning electron microscopic examination of periglacial eolian sands from Long Island, New York. *Journal of Sedimentary Research* 40, 1345–1350.
- Krinsley, D.H., Donahue, J., 1968. Environmental interpretation of sand grain surface textures by electron microscopy. *Geological Society of America Bulletin* 79, 743–748.
- Krinsley, D.H., Smalley, I.J., 1973. The shape and nature of small sedimentary quartz particles. *Science* 180, 1277–1279.
- Krinsley, D.H., Takahashi, T., 1962. Surface textures of sand grains: an application of electron microscopy. *Science* 135, 923–925.
- Li, C.X., Chen, Q.Q., Zhang, J.Q., Yang, S.Y., Fan, D.D., 2000. Stratigraphy and paleoenvironmental changes in the Yangtze Delta during late Quaternary. *Journal of Asian Earth Sciences* 18, 453–469.
- Liu, F., Li, G.J., Chen, J., 2014. U-Pb ages of zircon grains reveal a proximal dust source of the Xiashu loess, Lower Yangtze River region, China. *China Science Bulletin* 59, 2391–2395.
- Liu, T., Ding, Z., Rutter, N., 1999. Comparison of Milankovitch periods between continental loess and deep sea records over the last 2.5 Ma. *Quaternary Science Reviews* 18, 1205–1212.
- Lu, H.Y., An, Z.S., 1997. Paleoclimatic implication of grain-size distribution of loess at Luochuan. [In Chinese.] *Chinese Science Bulletin* 42, 66–69.
- Lu, H.Y., An, Z.S., 1998. Paleoclimatic significance of grain size of loess-paleosol sequences of central China. *Science in China, Series D: Earth Sciences* 41, 626–631.
- Machado, G.M.V., Albino, J., Leal, A.P., Bastos, A.C., 2016. Quartz grain assessment for reconstructing the coastal palaeoenvironment. *Journal of South American Earth Sciences* 70, 353–367.
- Mahaney, W.C., 2002. *Atlas of Sand Grain Surface Textures and Applications*. Oxford University Press, New York, pp. 1–237.
- Mahaney, W.C., Kalm, V., 2000. Comparative scanning electron microscopy study of oriented till blocks, glacial grains and Devonian sands in Estonia and Latvia. *Boreas* 29, 35–51.
- Mahaney, W.C., Stewart, A., Kalm, V., 2001. Quantification of SEM microtextures useful in sedimentary environmental discrimination. *Boreas* 30, 165–171.
- Mao, L., Mo, D., Li, M., Zhou, K., Yang, J., Guo, W., 2011. The rare earth element compositions of sediments from the loess tableland in the Liyang Plain, southern China: implications for provenance and weathering intensity. *Environment Earth Science* 62, 1609–1617.
- Margolis, S.V., Kennett, J.P., 1970. Antarctic glaciation during Tertiary recorded in sub-Antarctic deep sea cores. *Science* 170, 1085–1087.
- Margolis, S.V., Krinsley, D.H., 1974. Processes of formation and environmental occurrence of microfeatures on detrital quartz grains. *American Journal of Science* 274, 449–464.
- Newsome, D., Ladd P., 1999. The use of quartz grain microtextures in the study of the origin of sand terrains in Western Australia. *Catena* 35, 1–17.
- Nie, J., Stevens, T., Rittner, M., 2015. Loess plateau storage of northeastern Tibetan plateau-derived yellow river sediment. *Nature Communications* 6, 8511–8518.
- Paterson, G.A., Heslop, D., 2015. New methods for unmixing sediment grain size data. *Geochemistry, Geophysics, Geosystems* 16, 4494–4506.
- Pye, K., 1987. *Aeolian dust and dust deposits*. Academic Press, London.
- Qiao, Y.S., Hao, Q.Z., Peng, S.S., Wang, Y., Li, J.W., Liu, Z.X., 2011. Geochemical characteristics of the eolian deposits in southern China, and their implications for provenance and weathering intensity. *Palaeogeography, Palaeoclimatology, Palaeoecology* 308, 513–523.
- Qin, J., Wu, G., Zheng, H., Zhou, Q., 2008. The palynology of the first hard clay layer (late Pleistocene) from the Yangtze delta, China. *Review of Palaeobotany and Palynology* 149, 63–72.
- Sahu, B.K., 1964. Depositional mechanisms from the size analysis of clastic sediments. *Journal of Sediment Petroleum* 34, 73–83.
- Shi, Y.X., Dai, X.R., Song, Z.G., Yu L.Z., Guan, Z.Z., 2006. Particle size distribution and mineral components of atmospheric particles collected in spring of Shanghai. [In Chinese.] *Acta Sedimentologica Sinica* 5, 780–785.

- Song, Y.G., Zeng, M.X., Chen, X.L., Li, Y., Chang, H., An, Z.S., Guo, X.H., 2018. Abrupt climatic events recorded by the Ili loess during the last glaciation in Central Asia: evidence from grain-size and minerals. *Journal of Asian Earth Sciences* 155, 58–67.
- Strand, K., Passchier, S., Nasi, J., 2003. Implications of quartz grain microtextures for onset Eocene/Oligocene glaciation in Prydz Bay, ODP site 1166, Antarctica. *Palaeogeography, Palaeoclimatology, Palaeoecology* 198, 101–111.
- Sun, D., Bloemendal, J., Rea, D.K., Vandenberghe, J., Jiang, F., An, Z., Ruixia, S., 2002. Grain-size distribution function of polymodal sediments in hydraulic and aeolian environments, and numerical partitioning of the sedimentary components. *Sedimentary Geology* 152, 263–277.
- Sun, D.H., Lu H.Y., Rea D., 2000a. Bimode grain-size distribution of Chinese Loess and its paleoclimate implication. [In Chinese.] *Acta Sedimentologica Sinica* 18, 327–335.
- Sun, J.M., Ding, Z.L., Xia, X.P., Sun, M., Windley, B.F., 2018. Detrital zircon evidence for the ternary sources of the Chinese Loess Plateau. *Journal of Asian Earth Sciences* 155, 21–34.
- Sun, Y.B., Chen, H.Y., Tada, R., Weiss, D., Lin, M., Toyoda, S., Yan, Y., Isozaki, Y., 2013. ESR signal intensity and crystallinity of quartz from Gobi and sandy deserts in East Asia and implication for tracing Asian dust provenance. *Geochemistry, Geophysics, Geosystems* 14, 2615–2627.
- Sun, Y.B., Lu, H.Y., An, Z.S., 2000b. Grain size distribution of quartz isolated from Chinese loess/paleosol. *China Science Bulletin* 45, 2296–2298.
- Sun, Y.B., Lu, H.Y., An, Z.S., 2006. Grain size of loess, palaeosol and Red Clay deposits on the Chinese Loess Plateau: significance for understanding pedogenic alteration and palaeomonsoon evolution. *Palaeogeography, Palaeoclimatology, Palaeoecology* 241, 129–138.
- Tian, S.C., Sun, J.M., Gong, Z.J., 2017. Loess deposits in Beijing and their paleoclimatic implications during the last interglacial-glacial cycle. *Quaternary Science Reviews* 177, 78–87.
- Vandenberghe, J., 2013. Grain size of fine-grained windblown sediment: a powerful proxy for process identification. *Earth-Science Reviews* 121, 18–30.
- Vos K., Vandenberghe N., Elsen J., 2014. Surface textural analysis of quartz grains by scanning electron microscopy(SEM): from sample preparation to environmental interpretation. *Earth-Science Reviews* 128, 93–104.
- Wang, G., Li, J.R., Ravi, S., Pelt, R.S.V., Costa, P.J.M., Dukes, D., 2017a. Tracer techniques in aeolian research: approaches, applications, and challenges. *Earth-Science Reviews* 170, 1–16.
- Wang, J., Chen, G., Peng, Z., Grapes, R., 2015. Loess-like deposits in the Pearl River delta area, southeast China. *Aeolian Research* 19, 113–122.
- Wang, X., Wei, H.T., Khormali, F., Taheri, M., Kehl, M., Frechen, M., Luaer, T., Chen, F.H., 2017b. Grain-size distribution of Pleistocene loess deposits in northern Iran and its palaeoclimatic implications. *Quaternary International* 429, 41–51.
- Warrier, A.K., Pednekar, H., Mahesh, B.S., Mohan, R., Gazi, S., 2016. Sediment grain size and surface textural observations of quartz grains in late quaternary lacustrine sediments from Schirmacher Oasis, East Antarctica: paleoenvironmental significance. *Polar Science* 10, 89–100.
- Woronko, B., 2016. Frost weathering versus glacial grinding in the micromorphology of quartz sand grains: processes and geological implications. *Sedimentary Geology* 335, 103–119.
- Xia, F., Zhang, Y.Z., 2018. Late Quaternary strata and environmental evolution record of core LG in Longgang, north Jiangsu plain, China. [In Chinese.] *Geographical Research* 37, 433–446.
- Xiao, J.L., Porter, S.C., An, Z.S., Kumai, H., Yoshikawa, S., 1995. Grain size of quartz as an indicator of winter monsoon strength on the Loess Plateau of central China during the last 130,000 yr. *Quaternary Research* 43, 22–29.
- Xu, H.Y., Zheng, X.M., Zhou, L.M., 2016. Characteristics of quartz grains of the Xiashu loess in Zhoujiashan Nanjing and its provenance significance. [In Chinese.] *Acta Sedimentologica Sinica* 34, 1176–1186.
- Yamamoto, Y., Toyoda, S., Nagasima, K., Igarashi, Y., Tada, R., 2013. Investigation of the temporal change of the sources of aeolian dust delivered to East Asia using electron spin resonance signals in quartz. *Geochronometria* 40, 355.
- Yan, Y., Ma, L., Sun, Y.B., 2017. Tectonic and climatic controls on provenance changes of fine-grained dust on the Chinese Loess Plateau since the late Oligocene. *Geochimica et Cosmochimica Acta* 200, 110–122.
- Zhang, W., Chen, J., Ji, J., Li, G., 2016. Evolving flux of Asian dust in the North Pacific Ocean since the late Oligocene. *Aeolian Research* 23, 11–20.
- Zhang, W.F., Vleeschouwer, D.D., Shen, J., Zhang, Z., Zeng, L., 2018. Orbital time scale records of Asian eolian dust from the Sea of Japan since the early Pliocene. *Quaternary Science Reviews* 187, 157–167.
- Zhang, W.G., Yu, L.Z., Lu, M., Zheng, X.M., Shi, Y.X., 2007. Magnetic properties and geochemistry of the Xiashu loess in the present subtropical area of China, and their implications for pedogenic intensity. *Earth and Planetary Science Letters* 260, 86–97.
- Zhang, X.N., Zhou, A.F., Wang, X., Song, M., Zhao, Y.T., Xie, H.C., Russell, J.M., Chen, F.H., 2017. Unmixing grain-size distributions in lake sediments: a new method of endmember modeling using hierarchical clustering. *Quaternary Research* 89, 365–373.
- Zheng, X.M., 1999. *Aeolian Sediments and Environment in the Yangtze River Delta and the Adjacent Coastal Ocean*. [In Chinese.] East China Normal University Press, Shanghai.